DOI:10.1190/segam2020-3427988.1

A unique approach for estimating surface-wave instability and nonuniqueness

Julian Ivanov, Richard D. Miller, Anthony M. Hoch, Shelby L. Peterie, Sarah Morton, and Dmitry Borisov, Kansas Geological Survey*

Summary

We present a new method for estimating the nonuniqueness and/or instability of the seismic surface-wave method. This new approach uses a recently introduced objective function based on the secular function (i.e., a secular objective function [SOF]) for finding solutions to the Rayleigh surface-wave equation, focusing on very few model parameters (e.g., two). Initial research revealed the existence of a "nearly-exact-data nonuniqueness" valley with maximum fundamental-mode differences less than 3%. Another less pronounced valley (at ~60° with respect of the first one) required dispersion-curve picking errors to be less than 7-10% to minimize the effect of nonuniqueness. Results indicated that the new approach can expand the understanding of nonuniqueness or instability possibilities of the seismic surface-wave method. We think that the proposed method has the potential to significantly impact both practical applications and research on the seismic surface wave method.

Introduction

Estimation of shear-wave velocity (V_s) is important for the evaluation of stiffness properties in near-surface materials; V_s increases as material shear strength (rigidity) increases. The MASW method was initially developed to estimate near-surface shear-wave velocity from high-frequency (≥ 2 Hz) Rayleigh-wave data (Song et al., 1989; Park et al., 1998; Miller et al., 1999b; Xia et al., 1999b). Shear-wave velocities estimated using MASW have been reliably and consistently correlated with drill data. Using the MASW method, Xia et al. (2000) noninvasively measured V_s that were observed to be within 15% of V_s measured in wells. Miller et al. (1999b) mapped bedrock with 0.3-m (1-ft) accuracy at depths of about 4.5-9 m (15-30 ft), as confirmed by numerous borings.

The MASW method has been applied to problems such as characterization of pavements (Ryden et al., 2004), the study of Poisson's ratio (Ivanov et al., 2000a), study of levees and subgrade (Ivanov et al., 2004; Ivanov et al., 2006b), investigation of sea-bottom sediment stiffness (Ivanov et al., 2000b; Kaufmann et al., 2005; Park et al., 2005), mapping of fault zones (Ivanov et al., 2006a), study of Arctic ice sheets (Tsoflias et al., 2008; Ivanov et al., 2009), detection of dissolution features (Miller et al., 1999a), and measurement of V_s as a function of depth (Xia et al., 1999a). Applications of the MASW method have been extended to include determination of near-surface quality factor Q (Xia et al., 2013) and the acquisition of more realistic compressional-wave refraction models (Ivanov et al., 2006c; Ivanov et al., 2010; Piatti et al., 2013). A review of established surface wave methods (SWM) can be found in Socco et al. (2010) and ample textbook information can be found in (Foti et al., 2015). Most recent developments of the SWM include the expansion with the use of the horizontal component of the Rayleigh wave (Boaga et al., 2013), the simultaneous use of guided-waves with multi-mode surface waves in land and shallow marine environments (Boiero et al., 2013), evaluation at landfill sites (Suto, 2013), and use of the high resolution linear Radon transform (Ivanov et al., 2017a) to improve both the horizontal and linear resolution of the final 2D V_s models (Ivanov et al., 2017b).

The MASW method includes the following steps. A single seismic-data record (a.k.a. shot gather) is acquired. These data are transformed into a dispersion-curve image (Park et al., 1998; Luo et al., 2009), which is used to evaluate a dispersion-curve trend(s) of the Rayleigh wave. This curve is then inverted to produce a 1D V_s model (Xia et al., 1999b). By assembling numerous 1D V_s models, derived from consecutive seismic shot records, 2D (Miller et al., 1999b) or 3D (Miller et al., 2003) V_s models can be obtained.

Similar to other geophysical inverse problems, surface-wave inversion is mathematically ill-posed (Foti et al., 2015). Various degrees of both instability and/or nonuniqueness can be observed depending on the earth model parameters (Ivanov et al., 2013), assuming availability of accurate density and compressional-wave velocity (V_p) *a-priori* information. However, due to the lack of such *a-priori* information in many practical MASW applications and subsequent assumptions made, Ivanov et al. (2016) evaluated the impact of accurate density information on V_s inversion. As well, Ivanov et al. (2019) evaluated the influence of V_p *a-priori* information and its updates-during-the-inversion assumptions using real-world data.

Surface-wave instability and nonuniqueness evaluations include measuring dispersion-curve data sensitivity to model parameter changes (Liang et al., 2008) and obtaining numerous forward-modeling solutions using Monte Carlo inversion (Socco and Boiero, 2008). However, these approaches provide only a partial understanding of possible uncertainties in the final V_s results. They do not provide insights into nonuniqueness and instability specifics and range.

In efforts to broaden the understanding of surface-wave nonuniqueness and instability we chose to use a new approach, which takes advantage of a recently introduced new objective function (Yuefeng et al., 2019). It is a summed version of the Rayleigh secular function that uses numerous reference dispersion-curve data values (aka points) and modifies model

10.1190/segam2020-3427988.1

DOI:10.1190/segam2020-3427988.1

parameters to find appropriate secular objective function (SOF) minimums.

In this approach, we used a reference 10-layer reference model to calculate a fundamental-mode dispersion curve. As an initial step we chose to only modify the V_s value of layers 5 and 6 to scan for SOF minimums, which can be viewed as estimating a "local-model nonuniqueness". The resulting 2D image revealed two major bow-shaped nonuniqueness or instability valleys crossing each other at about 60 (120) degrees. The bow-shaped valley somewhat bent toward the axes minimums showed lower values than the other. Five points were selected to evaluate nonuniqueness. One at the approximate valleys' crossing point, representing the reference model and two more per valley. Each of the four latter SOF points represented a modified model. Corresponding fundamental and first five higher modes were calculate and compared with their counterparts from the reference model. Analysis showed that most of the points were almost an identical match to the referenced dispersion-curve points. The lower the SOF value the more dispersion-curve points had almost identical match not only for fundamental mode but for the higher modes as well.

Data

We used an arbitrary 10-layer model (Table 1) to calculate a reference fundamental-mode dispersion curve that would be used with the SOF calculations. In addition to the fundamental mode, the first five higher modes were calculated for a secondary analysis (Figure 1).

Table 1. The 10-layer model parameters used for the calculation of reference dispersion curves. "HS" stands for "Half-space"

Layer	V_s(m/s)	V_p(m/s)	Dens. (g/m^3)	Thick (m)
1	189.61	464.45	1.55	1.10
2	212.23	519.86	1.60	1.38
3	288.94	707.76	1.65	1.73
4	368.68	883.47	1.70	2.15
5	**460.65**	1128.35	1.75	2.69
6	**557.64**	1365.94	1.80	3.37
7	801.22	1962.58	1.85	4.21
8	897.58	2198.62	1.90	5.26
9	754.66	1848.52	1.95	6.57
10	740.66	1814.89	2.00	HS

Method

As a first step, we used the conventional dispersion-curve sensitivity calculations to identify some of the instability and nonuniqueness elements with the reference model. Dispersion-curve sensitivities were estimated by changing V_s of each layer by 10% and observing the percent frequency change in phase-velocity values for the fundamental-mode only (for brevity) (Figure 2). It can be noted that layers 9, 8, and 7 have very small influence on dispersion-curve values. Layer 6 through layer 2 show increased sensitivity in both amplitude and frequency-range width.

We propose another perspective for estimating possible nonuniqueness and instability using the SOF, introduced by Yuefeng et al. (2019). For that method, V_p, densities, layer thicknesses, and the calculated fundamental-mode dispersion curve from the reference model were kept constant and the V_s model was modified. For a selected 1D V_s model (i of M used), SOF$_i$ can be written as;

$$\boldsymbol{SOF_i = \frac{1}{N}\sum_j^N (F_j(f_j, c_{Rj}, \mathbf{v_{si}}, \mathbf{v_p}, \mathbf{d}, \mathbf{h}))} = 0,$$

(j = 1, 2, ..., N), where N is the number of dispersion-curve data points; f_j is the frequency and c_{Rj} the Rayleigh-wave phase velocity of each point; $\mathbf{v_{si}}$, $\mathbf{v_p}$, $\mathbf{d}$, and $\mathbf{h}$ are model vectors representing the layer parameters.

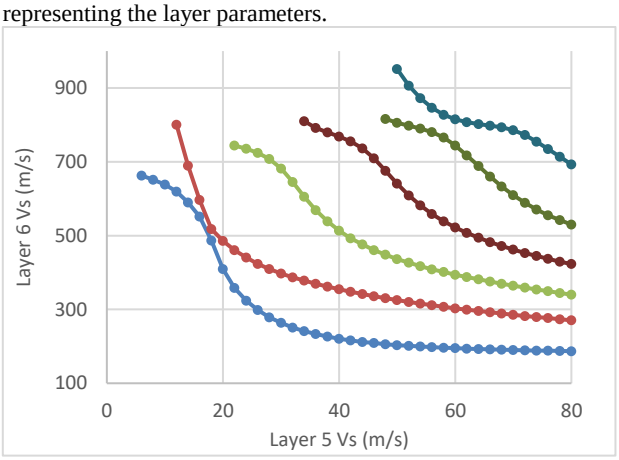

Figure 1. Calculated fundamental- and the first five higher mode (from bottom left to upper right) from Table 1 reference 10-layer model.

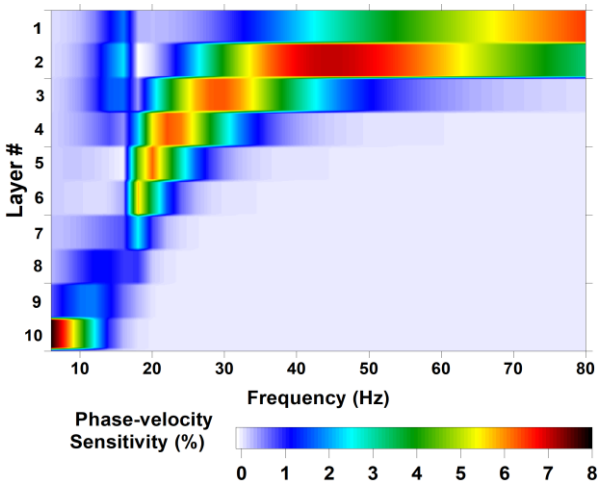

Figure 2. Rayleigh-wave fundamental-mode dispersion-curve sensitivity.

10.1190/segam2020-3427988.1

Two layers were selected as variable because of the greater focus and 2D visualization advantages. We chose the 5th and 6th layers (with 460.65 and 557.64 m/s values accordingly, Table 1) to examine for nonuniqueness and instability possibilities using a fundamental-mode-only SOF scan and a wider velocity range for both layers.

Results

Figure 3 displays a 2D SOF image generated by varying V_s between 415-570 m/s and 450-640 m/s for layers 5 and 6, respectively. A ~1.24 m/s velocity increment was chosen, which is ~0.2% of the maximum velocity (640 m/s). Two major bow-shaped minimum valleys can be observed crossing each other at about 60 (120) degrees. The bow-shaped valley with a steep trend down to the right showed lower values than the other, near horizontal curve.

Five points representing five different V_s models (because of the different V_s values for layers 5 and 6) were used from the 2D SOF image (Figure 4). First was the reference-model point (marked with a red circle on Figure 3; V_s5=460.65 and V_s6=557.64 m/s), which is positioned at the cross of the two valleys and had the lowest minimum value. Second was the point in the upper left, (marked with a red diamond V_s5=418.5 and V_s6=636.5 m/s). Third was another point from the greater-minimum valley (marked with a red square; V_s5=507 and V_s6=509 m/s) located at the lower right of the image.

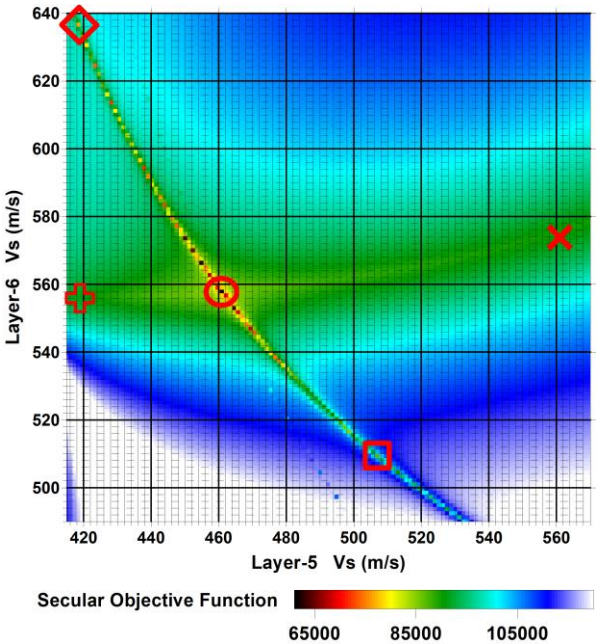

Figure 3. A SOF 2D image from scanning reference-model layers 5 and 6 *Vs* with ~1.24 m/s increment.

Fourth was a point from the moderate-minimum valley (marked with a red "X"; V_s5=561 and V_s6=574 m/s) at the right edge of the image. The fifth point was from the same moderate -minimum valley with a V_s5 almost identical to the V_s5 of the second point (marked with a red cross; V_s5=419 and V_s6=636.5 m/s) found at the left edge of the image (Figure 3). We calculated the fundamental and the first five higher modes using the above mentioned models 2-5 (Figure 4) and compared them with the corresponding modes from the reference model (Figure 5). Comparing the fundamental modes was given priority because usually the fundamental mode is the most interpretable, reliable, and widely used in the practical applications of the surface-wave method.

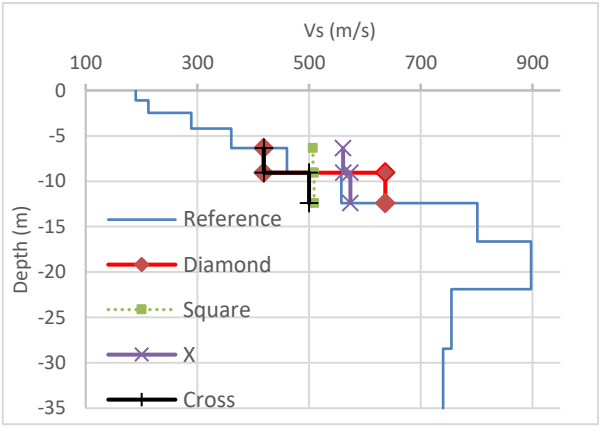

Figure 4. Plots of five velocity models a) the reference model from Table 1, V_s5=460.65 and V_s6=557.64 m/s (blue line), b) V_s5=418.5 and V_s6=636.5 m/s (red line with diamond marks), c) V_s5=507 and V_s6=509 m/s (green line and square marks), d) V_s5=561 and V_s6=574 m/s (purple line and X marks), and e) V_s5=419 and V_s6=556 m/s (blue line and cross marks)

Diamond and square fundamental-modes were practically a perfect match to the values given in the reference model. It is difficult to observe any difference looking at the equivalent graphs (Figure 5a and Figure 5b). The biggest difference in the diamond model was in the 20-26 Hz range at -2.3%, -2.62%, -2.08%, and -1.38% respectively while the rest were between 0-1%. The square model was very similar, with the corresponding numbers at -2.4%, -2.72%, -2.12%, and -1.35%.

The fundamental-modes from the cross (Figure 5c) and "X" (Figure 5d) models had somewhat bigger differences compared to the reference-model counterpart in the 18-26 Hz range, enough to be noticeable on the graphs. For the "X" model they were at -6.87%, -6.00%, -4.31%, -2.80%, and -1.66% respectively. The cross model mismatch points were above 1% in the 18-29 Hz range, with the largest difference at 5.60%, 14.41%, 10.29%, 6.10%, 3.26%, and 1.66%.

DOI:10.1190/segam2020-3427988.1

Factoring in the above information and considering the above observation to be representative for corresponding valleys, it can be hypothesized that there is a wide range of points within the lowest-minimum valley with a "nearly-exact-data nonuniqueness". On the other hand, uncertainties may exist along the moderate-minimum valley, if the dispersion-curve picking error in the ~18-26 Hz range is not below~7-10%.

Based on the four graphs in Figure 5, the possibility of using the first higher modes to resolve nonuniqueness or reduce uncertainties does not appear promising due to their almost perfect match with first higher mode of the reference model (numerical analysis not included for brevity). Most higher-mode 2 through 6 points, from the diamond (Figure 5a) and square (Figure 5b) models, were also a good match to the corresponding higher modes of the reference model, with very few exceptions mostly from the second mode. For the "X" (Figure 5c) and cross (Figure 5d) models more higher-mode (2 through 6) points could be used to resolve nonuniqueness, however, in practice it may be challenging to observe and/or interpret points from these higher modes.

Conclusions

We offer a new approach that can expand the understanding of nonuniqueness or instability possibilities of the seismic surface-wave method. Existing conventional Monte Carlo and sensitivity methods provide results, which may not be as informative as results from the approach described here. The Monte Carlo method makes a cloud of all-layer solution, which may not allow a thorough understanding. While the sensitivity method doesn't provide nonuniqueness or instability possibilities for a combinations of layers.

Acknowledgments

We also appreciate Mary Brohammer for her assistance in manuscript preparation.

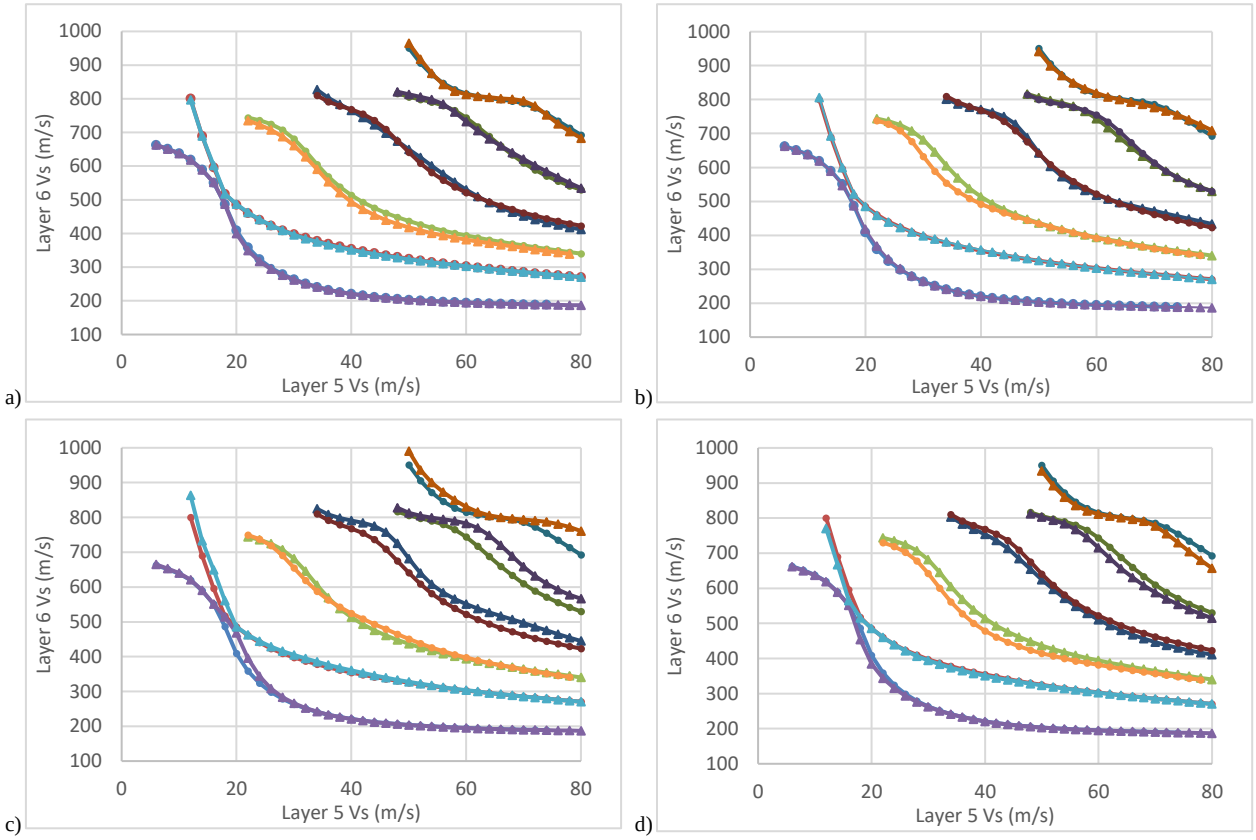

Figure 5. Matching fundamental-mode and the first five higher modes from each of the reference model (circle marks) to the corresponding curves of the modified models (triangle marks) a) *Vs5*=418.5 and *Vs6*=636.5 m/s (red diamond), b) *Vs5*=507 and *Vs6*=509 m/s (red square), c) *Vs5*=561 and *Vs6*=574 m/s (red X), and d) *Vs5*=419 and *Vs6*=556 m/s (red cross)

REFERENCES

Boaga, J., G. Cassiani, C. L. Strobbia, and G. Vignoli, 2013, Mode misidentification in Rayleigh waves: Ellipticity as a cause and a cure: Geophysics, **78**, EN17–EN28, doi: https://doi.org/ 10.1190/geo2012-0194.1.

Boiero, D., E. Wiarda, and P. Vermeer, 2013, Surface- and guided-wave inversion for near-surface modeling in land and shallow marine seismic data: The Leading Edge, **32**, 638–646, doi: https://doi.org/10.1190/tle32060638.1.

Foti, S., G. L. Carlo, G. J. Rix, and C. Strobbia, 2015, Surface Wave Methods for Near-Surface Site Characterization: CRC Press.

Ivanov, J., C. B. Park, R. D. Miller, and J. Xia, 2000a, Mapping Poisson's ratio of unconsolidated materials from a joint analysis of surface wave and refraction events: Symposium on the Application of Geophysics to Engineering and Environmental Problems, **13**, 11–19, doi: https://doi.org/10.4133/1.2922727.

Ivanov, J., C. B. Park, R. D. Miller, J. Xia, J. A. Hunter, R. L. Good, and R. A. Burns, 2000b, Joint analysis of surface wave and refraction events from river bottom sediments: 70th Annual International Meeting, SEG, Technical Program Expanded Abstracts, **19**, 1307–1310, doi: https://doi.org/10.1190/1.1815636.

Ivanov, J., R. D. Miller, R. F. Ballard, J. B. Dunbar, and J. Stefanov, 2004, Interrogating levees using seismic methods in southern Texas: 74th Annual International Meeting, SEG, Technical Program Expanded Abstracts, **23**, 1413–1416, doi: https://doi.org/10.1190/1.1851120.

Ivanov, J., R. D. Miller, P. Lacombe, C. D. Johnson, and J. W. Lane, 2006a, Delineating a shallow fault zone and dipping bedrock strata using multichannal analysis of surface waves with a land streamer: Geophysics, **71**, A39–A42, doi: https://doi.org/10.1190/1.2227521.

Ivanov, J., R. D. Miller, N. Stimac, R. F. Ballard, J. B. Dunbar, and S. Smullen, 2006b, Time lapse seismic study of levees in southern New Mexico: 76th Annual International Meeting, SEG, Technical Program Expanded Abstracts, 3255–3259, doi: https://doi.org/10.1190/1.2370207.

Ivanov, J., R. D. Miller, J. H. Xia, D. Steeples, and C. B. Park, 2006c, Joint analysis of refractions with surface waves: An inverse solution to the refraction-traveltime problem: Geophysics, **71**, R131–R138, doi: https://doi.org/10.1190/1.2360226.

Ivanov, J., G. Tsoflias, R. D. Miller, and J. Xia, 2009, Practical aspects of MASW inversion using varying density: Symposium on the Application of Geophysics to Engineering and Environmental Problems, **22**, 171–177, doi: https://doi.org/10.4133/1.3176692.

Ivanov, J., R. D. Miller, J. Xia, J. B. Dunbar, and S. L. Peterie, 2010, Refraction nonuniqueness studies at levee sites using the refraction-tomography and JARS methods:in R. D. Miller, J. D. Bradford, and K. Holliger, eds., Advances in near-surface seismology and ground-penetrating radar: SEG, **15**, 327–338, doi: https://doi.org/10.1190/1.9781560802259.ch20.

Ivanov, J., T. J. Schwenk, R. D. Miller, and S. Peterie, 2013, Dispersion-curve imaging nonuniqueness studies from multi-channel analysis of surface waves (MASW) using synthetic seismic data: SEG Technical Program Expanded Abstracts, 1794–1800, doi: https://doi.org/10.1190/segam2013-0425.1.

Ivanov, J., G. Tsoflias, R. D. Miller, S. Peterie, S. Morton, and J. Xia 2016, Impact of density information on Rayleigh surface wave inversion results: Journal of Applied Geophysics, **135**, 43–54, doi: https://doi.org/10.1016/j.jappgeo.2016.09.011.

Ivanov, J., R. Miller, D. Feigenbaum, and J. Schwenk, 2017a, Benefits of using the high-resolution linear Radon transform with the multichannel analysis of surface waves method: SEG Technical Program Expanded Abstracts **2017**, 2647–2653, doi: https://doi.org/10.1190/segam2017-17793766.1.

Ivanov, J., R. D. Miller, D. Feigenbaum, S. L. C. Morton, S. L. Peterie, and J. B. Dunbar, 2017b, Revisiting levees in southern Texas using Love-wave multichannel analysis of surface waves with the high-resolution linear Radon transform: Interpretation, **5**, T287–T298, doi: https://doi.org/10.1190/INT-2016-0044.1.

Ivanov, J., R. D. Miller, A. M. Hoch, S. L. Peterie, and S. Morton, 2019, Surface wave analysis sensitivity to a-priori information assumptions: SEG Technical Program Expanded Abstracts **2019**, 5030–5034, doi: https://doi.org/10.1190/segam2019-3216657.1.

Kaufmann, R. D., J. H. Xia, R. C. Benson, L. B. Yuhr, D. W. Casto, and C. B. Park, 2005, Evaluation of MASW data acquired with a hydrophone streamer in a shallow marine environment: Journal of Environmental and Engineering Geophysics, **10**, 87–98, doi: https://doi.org/10.2113/JEEG10.2.87.

Liang, Q., C. Chen, C. Zeng, Y. H. Luo, and Y. X. Xu, 2008, Inversion stability analysis of multimode Rayleigh-wave dispersion curves using low-velocity-layer models: Near Surface Geophysics, **6**, 157–165, doi: https://doi.org/10.3997/1873-0604.2007040.

Luo, Y. H., J. H. Xia, R. D. Miller, Y. X. Xu, J. P. Liu, and Q. S. Liu, 2009, Rayleigh-wave mode separation by high-resolution linear Radon transform: Geophysical Journal International, **179**, 254–264, doi: https://doi.org/10.1111/j.1365-246X.2009.04277.x.

Miller, R. D., J. Xia, C. B. Park, J. C. Davis, W. T. Shefchik, and L. Moore, 1999a, Seismic techniques to delineate dissolution features in the upper 1000 ft at a power plant site: 69th Annual International Meeting, SEG, Expanded Abstracts, **18**, 492–495, https://doi.org/10.1190/1.1821061.

Miller, R. D., J. Xia, C. B. Park, and J. M. Ivanov, 1999b, Multichannel analysis of surface waves to map bedrock: The Leading Edge, **18**, 1392–1396, doi: https://doi.org/10.1190/1.1438226.

Miller, R. D., T. S. Anderson, J. Ivanov, J. C. Davis, R. Olea, C. Park, D. W. Steeples, M. L. Moran, and J. Xia, 2003, 3D characterization of seismic properties at the smart weapons test range, YPG: 73rd Annual International Meeting, SEG, Technical Program Expanded Abstracts, **22**, 1195–1198, doi: https://doi.org/10.1190/1.1817493.

Park, C. B., R. D. Miller, and J. Xia, 1998, Imaging dispersion curves of surface waves on multi-channel record: 68th Annual International Meeting, SEG, Expanded Abstracts, 1377–1380, doi: https://doi.org/10.1190/1.1820161.

Park, C. B., R. D. Miller, J. Xia, J. Ivanov, G. V. Sonnichsen, J. A. Hunter, R. L. Good, R. A. Burns, and H. Christian, 2005, Underwater MASW to evaluate stiffness of water-bottom sediments: The Leading Edge, **24**, 724–728, doi: https://doi.org/10.1190/1.1993267.

Piatti, C., L. V. Socco, D. Boiero, and S. Foti, 2013, Constrained 1D joint inversion of seismic surface waves and P-refraction traveltimes: Geophysical Prospecting, **61**, 77–93. doi: https://doi.org/10.1111/j.1365-2478.2012.01071.x.

Ryden, N., C. B. Park, P. Ulriksen, and R. D. Miller, 2004, Multimodal approach to seismic pavement testing: Journal of Geotechnical and Geoenvironmental Engineering, **130**, 636–645. doi: https://doi.org/10.1061/(ASCE)1090-0241(2004)130:6(636).

Socco, L. V., and D. Boiero, 2008, Improved Monte Carlo inversion of surface wave data: Geophysical Prospecting, **56**, 357–371, doi: https://doi.org/10.1111/j.1365-2478.2007.00678.x.

Socco, L. V., S. Foti, and D. Boiero, 2010, Surface-wave analysis for building near-surface velocity models — Established approaches and new perspectives: Geophysics, **75**, 75A83–75A102, doi: https://doi.org/10.1190/1.3479491.

Song, Y. Y., J. P. Castagna, R. A. Black, and R. W. Knapp, 1989, Sensitivity of near surface shear wave velocity determination from rayleigh and love waves: 59th Annual International Meeting, SEG, Expanded Abstracts, **8**, 509–512, doi: https://doi.org/10.1190/1.1889669.

Suto, K., 2013, MASW surveys in landfill sites in Australia: The Leading Edge, **32**, 674–678. doi: https://doi.org/10.1190/tle32060674.1.

Tsoflias, G. P., J. Ivanov, S. Anandakrishnan, and R. D. Miller, 2008, Use of Active Source Seismic Surface Waves in Glaciology: Symposium on the Application of Geophysics to Engineering and Environmental Problems, **21**, 1240–1243, doi: https://doi.org/10.4133/1.2963234.

Xia, J., R. D. Miller, C. B. Park, J. A. Hunter, and J. B. Harris, 1999a, Evaluation of the MASW technique in unconsolidated sediments: 69th Annual International Meeting, SEG, Expanded Abstracts, 437–440, doi: https://doi.org/10.1190/1.1821046.

Xia, J., R. D. Miller, C. B. Park, J. A. Hunter, and J. B. Harris, 2000, Comparing shear-wave velocity profiles from MASW with borehole measurements in unconsolidated sediments, Fraser River Delta, B.C., Canada: Journal of Environmental and Engineering Geophysics, **5**, 1–13, doi: https://doi.org/10.4133/JEEG5.3.1.

Xia, J., C. Shen, and Y. Xu, 2013, Near-surface shear-wave velocities and quality factors derived from high-frequency surface waves: The Leading Edge, **32**, 612–618, doi: https://doi.org/10.1190/tle32060612.1.

Xia, J. H., R. D. Miller, and C. B. Park, 1999b, Estimation of near-surface shear-wave velocity by inversion of Rayleigh waves: Geophysics, **64**, 691–700, doi: https://doi.org/10.1190/1.1444578.

Yuefeng, Y., S. Chengyu, and L. Tengfei, 2019, The high-speed inversion of Rayleigh wave and its application analysis: SEG Technical Program Expanded Abstracts, 5010–5014, doi: https://doi.org/10.1190/segam2019-3215555.1.